Atmos. Chem. Phys. Discuss., https://doi.org/10.5194/acp-2018-564
Manuscript under review for journal Atmos. Chem. Phys.
Discussion started: 16 July 2018

Atmospheric Chemistry and Physics Discussions

Multi-Satellite Retrieval of SSA using OMI-MODIS algorithm

Kruthika Eswaran[1,2*], Sreedharan Krishnakumari Satheesh[1, 2] and Jayaraman Srinivasan[1, 2]

[1] Centre for Atmospheric and Oceanic Sciences, Indian Institute of Science, Bangalore, India

[2] Divecha Centre for Climate Change, Indian Institute of Science, Bangalore, India

**Correspondence to:* Kruthika Eswaran (kruthika.eswaran89@gmail.com)

Abstract - Single scattering albedo (SSA) represents a unique identification of aerosol type and aerosol radiative forcing. However, SSA retrievals are highly uncertain due cloud contamination and aerosol composition. Recent improvement in the SSA retrieval algorithm has combined the superior cloud masking technique of Moderate Resolution Imaging Spectroradiometer (MODIS) and the better sensitivity of Ozone Monitoring Instrument (OMI) to aerosol absorption. The combined OMI-MODIS algorithm has been validated over a small spatial and temporal scale only. The present study validates the algorithm over global oceans for the period 2008-2012. The geographical heterogeneity in the aerosol type and concentration over the Atlantic Ocean, the Arabian Sea and the Bay of Bengal was useful to delineate the effect of aerosol type on the retrieval algorithm. We also noted that OMI overestimates SSA when absorbing aerosols were present closer to the surface. We attribute this overestimation to data discontinuity in the aerosol height climatology derived from Cloud-Aerosol Lidar and Infrared Pathfinder Satellite Observations (CALIPSO) satellite. OMI uses pre-defined aerosol heights over regions where CALIPSO climatology is not present leading to overestimation of SSA. The importance of aerosol height was also studied using the Santa Barbara DISORT radiative transfer (SBDART) model. The results from the joint retrieval were validated with ground-based measurements and it was seen that OMI-MODIS SSA retrievals were better constrained than OMI only retrieval.

Atmos. Chem. Phys. Discuss., https://doi.org/10.5194/acp-2018-564
Manuscript under review for journal Atmos. Chem. Phys.
Discussion started: 16 July 2018

Atmospheric Chemistry and Physics Discussions

1. Introduction

Aerosols of different types are spatially distributed heterogeneously and at different altitudes in the atmosphere. Depending upon their properties, certain aerosols (biomass and carbon) warm the atmosphere by absorbing radiation, while other aerosols (sea salts and sulphates) cool the atmosphere by scattering radiation (Ramanathan et al., 2001). Due to the opposing effects on the atmosphere, aerosols can ~~have~~ either, net warming or cooling effect on the global climate depending upon the aerosol type, concentration and vertical distribution. Effect of aerosols on the global climate is measured by 'aerosol radiative forcing' (the perturbation to the earth's radiation budget caused by the presence of aerosols). Positive forcing implies atmospheric warming and vice-versa. (Liao and Seinfeld, 1998; Podgorny and Ramanathan, 2001; Satheesh, 2002; Johnson et al., 2003; Kim et al., 2004; Moorthy et al., 2004; Meloni et al., 2005; Satheesh and Moorthy, 2005; Seinfeld and Pandis, 2006; Satheesh et al., 2008; Chand et al., 2009; Mishra et al., 2015). According to the climate assessment report, the estimation of aerosol radiative forcing is a major cause of uncertainty in the estimation of climate sensitivity and therefore presents a great impediment to climate modeling (IPCC, 2013). The uncertainty is largely due to the lack of accurate measurement of the scattering and absorbing properties of the aerosols (Cooke and Wilson, 1996; Menon et al., 2002; Chung and Seinfeld, 2002; Bond and Sun, 2005).

The Single Scattering Albedo (SSA), (the fraction of radiation scattered out of total extinction of radiation) is used to distinguish the scattering and absorbing properties of aerosols. SSA represents a unique fingerprint of the type of aerosol and its radiative forcing (Hansen et al., 1997; Haywood et al., 1997; Myhre et al., 1998). In general, purely scattering aerosols have SSA value of approximately 1 while highly absorbing aerosols have SSA less than 0.7. However, SSA values lack high certainty (Bond and Bergstrom, 2006; Bond et al., 2013). Uncertainties in

SSA measurements are due to factors such as cloud contamination, instrumentation error and aerosol modification due to atmospheric processes. Better SSA retrievals (both in-situ and satellite-based) are required to reduce the uncertainty in SSA for a more accurate estimation of aerosol forcing; particularly over regions influenced by a variety of air masses. There is also a need for accurate spectral aerosol absorption measurements, which is required to validate SSA derived from satellite measurements (Bergstrom et al., 2007).

Studies on the various direct measurements of SSA and their uncertainty evaluation have been performed previously (Horvath, 1993, Heintzenberg et al., 1997; Moosmuller et al., 2009). Along with ground-based retrievals of SSA, there have been other indirect methods to retrieve the parameter using satellite images and observations (Table 1).

Though these previous studies on ground-based measurements have brought a fundamental understanding to the estimation of amounts of aerosols / aerosol chemistry, their restricted spatial and temporal extent is a major limitation. Moreover, these studies also have a reduced availability of scenes for indirect retrievals. Some techniques are limited due to cloud contamination while others operate only under specific conditions (e.g. presence of sun glint). This presents a need for better SSA retrieval algorithms that overcome the present technical limitations and that can be applied on a global scale. The global extent of observations from satellites has increased the spatial extent of the observations (Kaufman et al., 2002a). Though the satellite-based retrievals have been shown to be extremely successful over the majority of ocean and land regions, they still have a limited success over deserts and ice sheets. Over deserts and ice-sheets, high surface reflectance affects the satellite retrievals in visible spectrum. To counter this, SSA is retrieved in UV spectrum (330 nm to 400 nm) over these regions (Torres et al., 1998, 2007). In UV spectrum, the upwelling radiances are highly sensitive to the aerosol absorption

and also have a lower influence of surface albedo (Torres et al., 2007). SSA retrieval in UV spectrum also avoids difficulties encountered in scenarios where there are large surface reflectance contrasts.

The quality of OMI SSA retrievals is affected by sub-pixel cloud contamination and the spectral surface albedo (Torres et al., 2007). To counter the problems and uncertainties in the OMI SSA retrieval (Table 2), Satheesh et al. 2009 used retrieval from multiple satellites. They used combined retrieval from OMI-MODIS since ~~sensors on each of the satellites~~ have their own strengths and both fly within few minutes of each other in the A-train constellation (Stephens et al., 2002). The better cloud-screened retrieval of AOD from MODIS (Levy et al., 2003) and the high sensitivity of OMI to aerosol absorption were used to develop a hybrid algorithm to retrieve SSA (Satheesh et al., 2009). The study was performed over Atlantic Ocean and Arabian Sea for the year 2006. A comparison of the retrieved aerosol height with aircraft measurements showed that OMI-MODIS was more accurate than OMI. Gasso and Torres (2016) performed a detailed analysis of the OMI UV product retrievals over oceans and island sites. They compared the OMI retrieved AOD with MODIS and AERONET AODs. This work used the OMI-MODIS algorithm for only two particular cases over and near Africa to understand how the assumption of aerosol height and shape affected AOD and SSA retrievals. It was found that when the actual height from satellite Lidar was used instead of climatological values and when the shape of dust aerosols was assumed to be non-spherical, the retrievals by OMI agreed better with other observations including OMI-MODIS method. While the OMI-MODIS algorithm has been used in calculating aerosol radiative forcing (Satheesh et al., 2010) over oceanic regions surrounding India and used in retrieving SSA over land (Narasimhan and Satheesh, 2013) as well as used to understand the retrievals of OMI UV products for two particular cases (Gasso and Torres, 2016), a detailed

analysis of the algorithm on a larger spatial and temporal scale has not been done so far.

The current work applies the OMI-MODIS algorithm to retrieve SSA on a global scale. It is applied over global oceans from 2008-2012. Regional analysis over the Atlantic, the Arabian Sea and the Bay of Bengal has been done by incorporating the aerosol layer height and the type of aerosols. A simulation study using Santa Barbara DISORT Radiative Transfer (SBDART) model was performed to highlight the importance of aerosol layer height. After estimating SSA values using the OMI-MODIS algorithm, the present study then uses cruise measurements of SSA from the Integrated Campaign for Aerosols, Gases and Radiation Budget (ICARB) and winter ICARB campaigns over Arabian Sea and Bay of Bengal in 2006 and 2009 to validate the same (Moorthy et al., 2008, 2010).

2. Data

2.1. OMI

The Ozone Monitoring Instrument (OMI) on board the Aura satellite was launched in 2004. For OMI measurements two aerosol inversion schemes are used- OMI near UV (OMAERUV) algorithm and the multi-wavelength (OMAERO) algorithm (Torres et al., 2007). The OMAERO algorithm uses 19 wavelengths in the range of 330-500 nm to retrieve corresponding aerosol characteristics. For the present study we have used the OMAERUV algorithm which uses measurements at two wavelengths 354 nm and 388 nm. The reason behind choosing these wavelengths is the high sensitivity of upwelling radiances to aerosol absorption and the lower influence of surface in measurements due to low reflectance values in the UV region. This gives a unique advantage of retrieving aerosol properties over ocean and land including arid and semi-arid regions (Torres et al., 1998; 2007).

The products derived from the algorithm include AOD, absorption aerosol optical depth

(AAOD) and single scattering albedo (SSA). These are derived from pre-computed reflectance values for different aerosol models. Three major types of aerosols have been used - Desert dust, carbonaceous aerosols from biomass burning and sulphate-based aerosols. Each type has seven models of SSA. The retrieved products of OMAERUV are sensitive to the aerosol layer height (Torres et al., 1998). The values are derived at surface and at 1.5, 3.0, 6.0 and 10.0 km above the surface. The best estimate of the values of AOD, AAOD and SSA of a particular choice of aerosol vertical distribution are evaluated.

Due to the high sensitivity of SSA retrieval to the assumption of aerosol height and aerosol type, the OMI algorithm was improved (Collection 003-PGE V1.4.2, Torres et al., 2013) using climatology of aerosol layer height from CALIPSO (Cloud-Aerosol Lidar and Infrared Pathfinder Satellite Observations) along with carbon monoxide (CO) measurements from AIRS (Atmospheric Infrared Sounder) for better identification of carbonaceous aerosols. Torres et al. (2013) showed that the combined use of AIRS CO measurements and OMI Aerosol Index (AI) retrievals, helped in identifying the type of absorbing aerosol. Thus smoke layers were identified when values of AI and CO measurements were high and during events of high AI and low CO values, the aerosols were identified as dust. The AIRS CO measurements were also used to identify large aerosol loading which was otherwise represented as clouds by the OMAERUV algorithm. Using collocated observations of OMI and CALIOP, Torres et al. (2013) estimated the height of elevated absorbing aerosols for a 30-month period from July 2006 to December 2008. An effective aerosol height was calculated from the attenuated backscatter weighted with average height using the CALIOP 1064 nm measurements. The 30-month climatology of aerosol height was used in the OMAERUV algorithm and validated with Aerosol Robotics Network (AERONET) observations (Torres et al., 2013). The results showed that there was improvement

Atmos. Chem. Phys. Discuss., https://doi.org/10.5194/acp-2018-564
Manuscript under review for journal Atmos. Chem. Phys.
Discussion started: 16 July 2018

in the retrievals. The original aerosol height assumptions were used in the algorithm over regions where the climatology was unavailable. For the present study we have used the improved OMAERUV algorithm along with AOD, SSA retrievals at different aerosol heights and as well as the best estimates of AOD and SSA.

2.2. MODIS

The Moderate Resolution Imaging Spectrometer (MODIS) instrument ~~in~~ Aqua satellite was launched in 2002. This instrument, with 36 spectral channels has a unique ability to retrieve aerosol properties with better accuracy over both land and ocean (Remer et al., 2005; Levy et al., 2003). Of these, seven channels (0.47-2.13 μm) are used to retrieve aerosol properties over ocean (Tanre et al., 1997).

As described in Remer et al., (2005), before the retrieval algorithm, masking of sediments, clouds and ocean glint is performed to separate valid pixels from bad ones. The retrieval algorithm of MODIS (also called the inversion procedure) has been described in detail previously (Tanre et al., 1997; Levy et al., 2003; Remer et al., 2005). The algorithm uses a 'look-up table' (LUT) approach, i.e., for a set of aerosol and surface parameters, radiative transfer calculations are performed. Spectral reflectance derived from the LUT is compared with MODIS-measured spectral reflectance to find the 'best' (least-squares) fit. The resulting combination of modes provides the aerosol model from which size distribution, properties including spectral optical depth, effective radius etc. ~~is~~ derived. The product used from MODIS is the Level 2 aerosol (MYD04, Collection 5.1) product. The parameter chosen is 'Effective_Optical_Depth_Average_Ocean' which provides the aerosol optical depth over ocean at seven wavelengths. The value is the average of all the solutions in the inversion procedure with the least-square error < 3%.

Atmos. Chem. Phys. Discuss., https://doi.org/10.5194/acp-2018-564
Manuscript under review for journal Atmos. Chem. Phys.
Discussion started: 16 July 2018

A combination of OMI and MODIS helps indirectly in counteracting the cloud contamination problem and also uses the strength of the individual sensors – OMI's sensitivity to aerosol absorption combined with the better cloud screening of MODIS and accurate retrieval of AOD, and aerosol size (Satheesh et al., 2009; Narasimhan and Satheesh, 2013).

3. Algorithm

MODIS has high spatial pixel resolution of 10km x 10km at nadir (and a cloud mask at 500m and 1km resolution) whereas OMI has a resolution of 13 km x 24 km. This results in a pixel being prone to cloud contamination which overestimates AOD and underestimates single scattering co-albedo (1-SSA) (Torres et al., 1998). However, AAOD can be retrieved in the presence of small cloud contamination since there is cancellation of errors (Torres et al., 2007).

The higher accuracy in MODIS retrieval over ocean is due to the fact that it has large number of channels in the Shortwave Infrared (SWIR) region (Tanre et al., 1997; Remer et al., 2005; Levy et al., 2003). While OMI is highly sensitive to aerosol absorption in the near-UV region, the accuracy in the retrieval of AAOD depends on the aerosol layer height assumption. OMI provides AOD and AAOD at different heights as prescribed by various aerosol types (Torres et al., 2007).

The assumption of aerosol layer height in the OMI algorithm restricts the retrieval of AOD and AAOD. Using this as basis, the approach proposed in Satheesh et al. (2009) used MODIS AOD as an input to the OMI retrieval algorithm, so that the ~~inversion, now checked, can use the information~~ to infer the aerosol layer height and SSA. ~~To know the SSA at 388 nm, the AOD used should also be at the same wavelength.~~ Satheesh et al. (2009) extrapolated MODIS AOD and compared the estimated UV AOD with high quality ground-based AERONET observations. The deviation between ~~MODIS~~-extrapolated AOD and AERONET AOD was greater at higher

AERONET AOD values. This was attributed to the presence of large number of fine-mode aerosols which affected AOD at UV wavelengths. Hence to improve the linear extrapolation, information on the aerosol spectral curvature was also included. This was achieved by using an average regression equation to correct the MODIS AOD (Satheesh et al., 2009; Equation 3). They showed that MODIS AOD can be linearly extrapolated to 388 nm and ~~use the~~ corrected ~~AOD~~ as input to the OMI retrieval algorithm. The present work uses the same algorithm as proposed by Satheesh et al. (2009) to retrieve SSA over the oceans for the region 60S-60N and 180W-180E from December 2007-November 2012. The methodology is described in detail in the following section.

4. Methodology

The AOD for ocean obtained from the Level 2 aerosol product of MODIS (MYD04) was used. Using linear extrapolation, AOD at 388 nm (hereafter, AOD_{388}) was calculated from AOD at seven wavelengths ranging from 0.47-2.13 ~~μm, after the inclusion of aerosol spectral curvature defined in Satheesh et al. (2009)~~. OMI provides AOD and SSA for five different aerosol layer heights starting from surface and at 1.5, 3.0, 6.0 and 10.0km (AOD_{omi} and SSA_{388}). It also provides the best estimate of SSA calculated for a particular aerosol vertical distribution (SSA_{omi}).

For the present study, polar regions are not included and hence pixels from both OMI and MODIS that are outside the 60S-60N and 180W-180E region are excluded. Pixels with invalid or missing values are also excluded. To reduce computation time the various parameters extracted from the data were re-gridded onto a uniform grid of 0.5˚ x 0.5˚ within the region of study. For both the satellites, this procedure was repeated for each swath data which were then combined to calculate the daily means.

Atmos. Chem. Phys. Discuss., https://doi.org/10.5194/acp-2018-564
Manuscript under review for journal Atmos. Chem. Phys.
Discussion started: 16 July 2018

Atmospheric Chemistry and Physics Discussions

The daily data from collocated MODIS and OMI were utilised in the final algorithm. As mentioned before OMI provides AOD and SSA for five different aerosol layer heights. Using AOD_{388} as the reference, the corresponding aerosol layer height was calculated from the five AOD_{omi} values through linear interpolation. This height is then used as a reference to find the SSA using interpolation from the set of SSA_{388} values. Finally, this SSA ($SSA_{omi\text{-}modis}$), and the best estimate of SSA (SSA_{omi}) were compared ~~to~~ each other.

5. Results

The spatial distribution of SSA retrieved using OMI is shown in Fig. 1a. The values are averaged over five years and plotted seasonally.

The SSA retrieved using OMI-MODIS algorithm is shown in Fig. 1b.

SSA over open oceans is close to 1 due to the presence of large amount of sea-salt and sulphate. Closer to land, a variety of aerosols are present which results in SSA varying from 0.75 to ~1. Over the oceans, separating ocean colour effects and aerosol concentrations is difficult. Hence the OMI algorithm retrieves only if there are enough absorbing aerosols present, i.e.AI >=0.8 (Torres et al., 2013). Only pixels whose quality has been assigned as 0 or the highest quality by OMI have been used. Since 2007, observations have been affected by a phenomenon called the *row anomaly* which reduces the quality of radiance at all wavelengths. The points flagged for row anomaly are not used in this study. Further information about row anomaly can be found in Jethva et al. (2014). Thus, the retrievals did not cover the entire globe. From Fig.1a it can be seen that majority of the valid SSA retrievals were over major aerosol sources in the world and not over remote oceanic regions like central equatorial Pacific or Antarctic ocean. The major sources include the vast biomass outflow over Atlantic Ocean from the west coast of Africa, the dust over Arabian Sea from the arid areas of Arabia & Africa and the dust blown over

Atmos. Chem. Phys. Discuss., https://doi.org/10.5194/acp-2018-564
Manuscript under review for journal Atmos. Chem. Phys.
Discussion started: 16 July 2018

Atlantic Ocean from Sahara. Other regions like the east coast of China, Bay of Bengal are influenced by a variety of anthropogenic aerosols during different seasons. Both the algorithms capture the major oceanic regions which are influenced by large number of aerosols.

Two important regions over oceans influenced by a variety of aerosols are the Atlantic Ocean and the oceans around the Indian subcontinent. The new approach was used over these regions- Atlantic (5N-30N; 60W-20W) (ATL) and Arabian Sea and Bay of Bengal (0-25N; 55E-100E) (ARBOB).

5.1. Difference in SSA retrieval algorithms during different seasons

To understand how the OMI-MODIS algorithm compared with the retrieval using existing OMI algorithm, the difference between $SSA_{omi\text{-}modis}$ and SSA_{omi} (ΔSSA) averaged over five years for different seasons is shown in Fig. 2.

During March-April May (MAM) and June-July-August (JJA), there is a longitudinal gradient in ΔSSA from the coast of Sahara towards the open Atlantic Ocean. Kaufman et al. (2002a) showed that closer to the coast of Africa, aerosols are more absorbing than those away from the coast. The difference in the type of aerosols as we move away from the coast could be one of the reasons for the gradient in ΔSSA. The ΔSSA changes sign with season. This was attributed to the dominating presence of either natural aerosols (JJA) or anthropogenic aerosols (DJF).

Both ATL and ARBOB regions are influenced by the type of aerosols which result in a complex mixture and eventually resulting in the variation in SSA distribution over each season. While the spatial plot of ΔSSA in Fig. 2 represents the regions where maximum and minimum differences are located around the globe, a distribution plot provides the ranges of ΔSSA which dominate and which do not. The distribution of ΔSSA for different seasons averaged over five

253 years (2008-2012) is plotted in Fig. 3a and 3b for the regions- ATL and ARBOB respectively.

254 DJF shows a strong positive bias in both the regions, JJA shows a negative bias and the
255 other two seasons show negligible bias. While dust outflows dominate over ATL, over ARBOB –
256 Arabian Sea is affected by dust at higher altitudes and sea-salt near the surface whereas the Bay
257 of Bengal is influenced mainly by continental and marine aerosols. The change in the sign of
258 difference could either be due to the difference in type of aerosol or the assumption in aerosol
259 layer height (ALH). To understand what type of aerosols affect these water bodies, trajectory
260 analysis is done. This helps in identifying major sources of aerosols during each season.

261 **5.2. Trajectory analysis**

262 **5.2.1. Atlantic (ATL)**

263 The region in the tropical Atlantic is surrounded by the Sahara Desert in the east and the
264 North America in the west. The transport of dust from Sahara over Atlantic Ocean is a regular
265 occurrence (Prospero and Carlson, 1972). Aerosol distribution over Atlantic is also affected by
266 the African Easterly Waves and other atmospheric dynamics in Africa (Zuluaga, 2012). The
267 Atlantic region is influenced by not only dust from Sahara, but also by aerosols from biomass
268 burning ~~off the coast of~~ Africa and aerosols from ~~industries and pollution~~ from ~~America~~. Thus,
269 there is a complex mixture of aerosols over the Atlantic Ocean during any season. A 7-day back
270 trajectory analysis was performed at a location in the box (15N; 45W) using the online Hybrid
271 Single-Particle Lagrangian Integrated Trajectory (HYSPLIT) model for the years 2009-2010.
272 The trajectory was computed for different seasons at 3 heights – 500m, 1500m and 2500m above
273 mean sea level (MSL). The Atlantic Ocean was divided into four quadrants representing the
274 regions of possible sources of aerosols 1) North America, 2) Central/South America, 3) North
275 Africa and 4) ~~Southern~~ Africa (Fig. 4). The influence of these aerosol sources over Atlantic

Atmos. Chem. Phys. Discuss., https://doi.org/10.5194/acp-2018-564
Manuscript under review for journal Atmos. Chem. Phys.
Discussion started: 16 July 2018

Ocean is estimated as the percentage of trajectories that start from each region respectively. The maximum influence is given in bold (Table 2).

From Table 2 it can be seen that the major source of aerosols over the Atlantic Ocean is the dust outflow from the Sahara Desert (Prospero, 1996). Extreme heating over Sahara creates a layer of instability (Saharan Air Layer) which lifts the dust particles enabling long-range transport. Far off the coast the warm dust layer encounters a cooler, wetter air layer causing inversion. This results in the dust layer ~~being~~ intact over Atlantic Ocean (Prospero and Carlson, 1972). Field experiments like the trans-Atlantic Aerosol and Ocean Science Expeditions (AEROSE I and II) showed the outflow of dust during spring and summer along with other trace gases and biomass aerosols (Morris et al., 2006). However, dust is not the only aerosol present in the region of study. Using an airborne differential absorption LIDAR (DIAL) system, Harriss et al. (1984), found that there is advection of anthropogenic pollutants from North America to the North Atlantic Ocean. Advanced very high-resolution radiometer (AVHRR) instrument on the National Oceanic and Atmospheric Administration (NOAA) 11 satellite provides global aerosol information. From that data it was found that large plumes over Atlantic Ocean were attributed to the pollution from North America and Europe. During spring and summer, the large outflow was due to the dust outbreak from Sahara and Sahel. Biomass burning from southern Africa, South America and anthropogenic emissions from North and Central America dominated the aerosol loading over Atlantic Ocean during winter (Husar et al., 1997). The MODIS instrument onboard the Terra satellite was first used to study the transport and deposition over Atlantic Ocean. It was found that during winter, the dust which was present was mixed with the biomass aerosols from Sahel and closer to the coast of North America the dust was influenced by the pollution and smoke from the continent. Pure dust was present over the ocean during summer months

299 (Kaufman et al., 2005). From Table 2 it is also seen that the dust dominated at all heights except
300 during winter when the pollution from North America dominated at higher altitudes.

301 **5.2.2. Arabian Sea and Bay of Bengal (ARBOB)**

302 The Arabian Sea and the Bay of Bengal are oceanic regions on the west and east coast of
303 India respectively. Both regions are influenced by various types of aerosols during different
304 seasons. The Arabian Sea has been dominated by dust aerosols and is influenced by high levels
305 of dust during certain seasons as seen from satellite images (Sirocko and Sarnthein, 1989). Pease
306 et al. (1998) studied the geochemistry and the transport of various dust samples during different
307 cruises in different seasons. During winter and summer, the pattern of aerosol transport was
308 similar to that of the Indian monsoon pattern – northeasterly (winter) and southwesterly
309 (summer). Thus, the major sources of aerosols were the Arabian Peninsula (including Saharan
310 dust and Middle East) and Indian sub-continent in summer and winter respectively. The mean 7-
311 day back trajectory using HYSPLIT model from a point over Arabian Sea (15N; 65E) was
312 performed for each season of 2010 and at three different heights (500m, 1500m and 2500m
313 above MSL). Only one year is performed since the trajectory analysis over Atlantic Ocean
314 showed that the aerosol pathways did not vary much between years. The Arabian Sea region was
315 divided into four quadrants – 1) Arabian Peninsula and North Africa, 2) ~~Southern~~ Africa, 3)
316 Indian sub-continent and 4) Indian Ocean and Southeast Asia (Fig. 5). Similar to Table 2,
317 influence of different aerosol source regions over the Arabian Sea is given in Table 3.

318 Similar to Pease et al. (1998), Tindale and Pease (1999) found that transport of aerosols near
319 the surface followed the surface wind currents. The dust content was low near the surface during
320 summer due to the presence of Findlater jet, but the general dust concentrations were higher than
321 other oceanic regions. During winter, the winds are predominantly north and north easterly and

hence results in transport of aerosols from India/Pakistan/Afghanistan onto Arabian Sea. However, the presence of anticyclonic circulation over Arabia (20N; 60E) results in north westerly winds transporting dust over Arabian Sea (Rajeev et al., 2000). The spring time (March-April-May) is the transition between northeast and southwest monsoon. The winds become south westerlies which result in the advection of aerosols from open Indian Ocean or near Somalia. At higher altitudes (above the Findlater jet) dust transport occurs from Arabia. During summer, the southwest monsoon wind patterns carry aerosols all the way from southeast/east Indian Ocean (mainly sea-salt). As the altitude increases, the wind patterns change a little due to aerosols coming from southwest Indian Ocean/Somalia. Above the Findlater jet, as explained by Tindale and Pease (1999), dust transport occurs from Arabian Peninsula (Table 3).

Being an integral part in the Indian Summer Monsoon, studies over Bay of Bengal is important especially the role of aerosols in the local climate change. While Arabian Sea is dominated by dust and oceanic aerosols and only anthropogenic aerosols during SON, studies have shown that Bay of Bengal is influenced by various air masses associated with Asian monsoon system (Krishnamurti et al., 1998). The synoptic meteorological conditions over Bay of Bengal have been studied in detail by Moorthy et al. (2003) and Satheesh et al. (2006). Similar to the other two regions, mean 7-day back trajectory analysis from a point over (15N; 90N) was performed for each season of 2010 and at three different heights (500m, 1500m and 2500m above MSL). The four quadrants representing the various aerosol source regions are 1) India/Arabian Peninsula, 2) Indian Ocean, 3) North/Northeast India and East Asia and 4) Southeast Asia (Fig. 6). Table 4 represents the influence of aerosol source regions over Bay of Bengal.

The north westerly winds occur from west to east in the Indo-Gangetic Plain (IGP) and due

to subsidence, the aerosols are trapped in the east during winter (Dey and Di Girolamo, 2010; Di Girolamo et al., 2004). The IGP with its heavy population and large number of industries acts as a source for anthropogenic aerosols which are transported to Bay of Bengal during winter (Kumar et al., 2013). Along with mineral dust from Arabian Peninsula, biomass aerosols from Southeast Asia are also transported to the bay. Field experiments like ICARB (Moorthy et al., 2008) during the spring time (pre-monsoon) showed transports of aerosols from the Arabian Peninsula and also presence of elevated aerosols (anthropogenic and natural) over Bay of Bengal (Satheesh et al., 2008). The post monsoon season acts as a transition from the summer to winter monsoon. The winds during September are still south westerlies and during October weak westerlies are present (Lawrence and Lelieveld, 2010). This results in transportation of aerosols from Indian Ocean and Arabian Sea. Thus, from Table 4 it can be seen that both anthropogenic aerosols (from IGP, Southeast Asia) and natural aerosols (marine and dust) are present over Bay of Bengal during different seasons.

5.3. Role of Aerosol Layer Height in SSA retrieval

Satheesh et al. (2009) devised a new algorithm to improve the retrieval of SSA using combined OMI and MODIS data. They used MODIS-predicted UV AOD as the input to improve the original OMI algorithm, which was constrained by the assumption of aerosol layer height. Over the Atlantic, the values retrieved from both algorithms showed reasonably good agreement. However, over the Arabian Sea only when there was considerable loading of dust, the OMI AOD and MODIS AOD had agreement suggesting that during other seasons, the assumption of aerosol height could be wrong. Satheesh et al. (2009) also found that over Arabian Sea the aerosol layer height (ALH) derived from OMI-MODIS algorithm agreed well with aircraft measurements when compared to OMI SSA retrieval. In the current work, the aerosol layer height (ALH) was

368 calculated for OMI, using the best estimate of SSA retrieved from OMI. The difference in
369 aerosol layer height between OMI-MODIS and OMI was plotted with the difference in SSA (Fig.
370 7a and 7b). The colorbar in the figure represents height estimated using the OMI-MODIS
371 algorithm.

372 Most important observation from this analysis is that OMI overestimates SSA at lower ALH
373 (retrieved by OMI-MODIS algorithm) and underestimates SSA at higher ALH. The latest version
374 of OMI algorithm uses CALIPSO climatology of aerosol layer height for better accuracy.
375 However, over regions where this is not available, pre-defined aerosol height has been used
376 based on the type of aerosol assumed. For industrial sulphate aerosols exponential profile with
377 2km scale height is assumed with a similar profile with 1.5km scale height for oceanic aerosols.
378 For biomass type aerosols, a Gaussian distribution with peak at 3km is used. Dust aerosols are
379 assumed to have two-single Gaussian distributions with maximum at heights 3 and 5km. It has
380 been shown by Gasso and Torres (2016) that when the actual aerosol height was 1.5km more
381 than climatological or assumed height, OMI retrieved higher SSA.

382 It can be seen from Figs. 7a and 7b, the blue coloured circles represent height between
383 surface to ~ 2km. In this range it is seen that the height assumed by OMI is > 1.5km compared to
384 the one estimated by OMI-MODIS. Thus, OMI overestimates SSA compared to the OMI-
385 MODIS retrieval. This overestimation is due to the predefined vertical profiles. Thus, there are
386 errors with regard to both the aerosol layer height as well as the type of aerosol in the OMI
387 algorithm. In the OMI algorithm, the highest uncertainty in retrieving SSA is due to aerosol layer
388 height and aerosol type (Torres et al., 2002). Using ground-based LIDAR measurements,
389 Satheesh et al. (2009) concluded that OMI-MODIS retrieved height agreed better with
390 observations than OMI.

Atmos. Chem. Phys. Discuss., https://doi.org/10.5194/acp-2018-564
Manuscript under review for journal Atmos. Chem. Phys.
Discussion started: 16 July 2018

The importance of ALH and SSA in the calculation of TOA flux is studied using Santa Barbara DISORT (SBDART) model (Ricchiazzi et al., 1998). For the same tropical environment variables and surface albedo of 0.06, the SSA was varied from 0.8 to 1 and aerosol height from 0 to 10 km at 1 km interval. The simulations were done for a narrow band in UV (300-400nm). For a constant AOD, AE (Angstrom Exponent) and asymmetry factor (0.4, 1 and 0.7 respectively), TOA flux was calculated (Fig. 8). It can be seen that at any ALH, TOA flux varied with SSA in. The role of ALH is important in the UV region due to the phenomena of Rayleigh scattering (van de Hulst, 1981). The importance of Rayleigh scattering on the role of ALH is further shown in Fig. 9. In this particular set of simulations, the Rayleigh scattering is completely removed and all other parameters are kept same as in Fig. 8.

It can be seen that once molecular scattering is removed, the effect of ALH is also removed and TOA flux depends only on SSA and other aerosol properties. This set of SBDART simulations shows us how for a particular value of TOA flux, assuming different aerosol height gives us different SSA values reiterating the important role of aerosol height on SSA retrievals.

5.4. Validation

To validate the new retrieval method of SSA using OMI and MODIS, both SSA values from OMI and OMI-MODIS were compared with ground-based measurements (SSA at 450nm) during ~~Cruises~~ in the period 2006 and 2009 in Arabian Sea and Bay of Bengal. These cruises were part of the Integrated Campaign for Aerosols, gases and Radiation Budget (ICARB) performed during the months of March to May 2006 and once during winter (W-ICARB) from 27 December 2008 to 30 January 2009 (Moorthy et al., 2008 and 2010). Since the spatial coverage of OMI-MODIS and cruise measurements ~~is less~~, the SSA values for both the algorithms were averaged over the region of study and compared with observed SSA (Fig. 10).

However, the cruise measurements showed that SSA varied a lot spatially especially over Bay of Bengal. Hence instead of a spatial average, the SSA values were temporally averaged for the months when the cruise was performed. This was done under the assumption that during the cruise period, the SSA over each location did not vary with time. For better coverage, a 1.5^{o} box was used around each location within which the mean SSA was calculated.

The mean SSA of OMI, OMI-MODIS and cruise measurements are calculated and the difference between mean satellite SSA and mean SSA from cruise measurements are calculated for OMI and OMI-MODIS algorithms separately. A statistical t-test is performed comparing the respective SSA means of OMI and OMI-MODIS with SSA. The null hypothesis assumes the mean SSA of OMI/OMI-MODIS is equal to the mean SSA calculated from the cruise measurements. The values from Table 5 show that despite the mean difference of OMI SSA and cruise SSA being ~ 0.013, it was statistically significant at 95% significance level. On the other hand the SSA retrieved using OMI-MODIS algorithm was better constrained and was closer to the mean value of SSA from cruise measurements. The distribution of SSA from both the satellite algorithms as well as from cruise measurements is shown in Fig. 11.

Using five years (2008-2012) of OMI and OMI-MODIS data for the region of Arabian Sea and Bay of Bengal, SSA was retrieved and the difference between the two methods was calculated and plotted against SSA from the OMI-MODIS algorithm (Fig. 12). For absorbing aerosols detected by OMI-MODIS the SSA is overestimated by OMI.

The OMI-MODIS approach in SSA retrieval is one of the many combinations of sensors that can be used in retrieving aerosol properties. A more complete approach involving better vertical distribution of aerosols either from space or ground-based observations is required to reduce the uncertainty further. However, with few ground-based measurements in the UV regime, validation

437 of new algorithms is still in the nascent stage.

438 **6. Summary and Conclusions**

439 Aerosol forcing depends on aerosol properties like aerosol optical depth (AOD) and single
440 scattering albedo (SSA). SSA is highly sensitive to the aerosol composition and size and as well
441 as the wavelength at which the aerosol interacts with radiation. A slight change in SSA value can
442 alter the sign of the forcing. Hence it is important to have an accurate measurement of SSA
443 globally. Ozone Monitoring Instrument (OMI) retrieves SSA in the UV spectrum. However,
444 these retrievals are affected by cloud contamination and are sensitive to aerosol layer height. To
445 resolve the issue of sub-pixel cloud contamination, Satheesh et al (2009) developed a method
446 using the combination of OMI and the Moderate Resolution Imaging Spectroradiometer
447 (MODIS) at a local scale. In the present study, we use the method developed by Satheesh et al
448 (2009) to retrieve SSA at a much larger spatial and temporal scale. The main findings from our
449 study are listed below:

450 1. Both OMI and OMI-MODIS algorithms retrieved SSA over regions influenced by large
451 amounts of aerosols (e.g. Atlantic Ocean – ATL; Arabian Sea and Bay of Bengal –
452 ARBOB)
453 2. Difference in SSA retrievals of OMI-MODIS and OMI for both regions ATL and
454 ARBOB fluctuates between positive and negative values during different seasons which
455 could be due to the difference in either the type of aerosol or aerosol height assumed. In
456 addition, a longitudinal gradient of difference in SSA retrievals is present from the coast
457 of Sahara to the open ocean during the JJA season. This could be due the difference in
458 type of aerosols near the coast and in the open ocean
459 3. OMI overestimates SSA at lower ALH and underestimates at higher values of ALH. Over

regions where CALIPSO climatology is not present, OMI uses pre-defined aerosol heights based on the aerosol present. From Fig. 4 it is also seen that OMI is unable to retrieve absorbing aerosols present at very low heights (< 2km) due to the already defined vertical profiles.

4. In the UV spectrum, ALH plays a more dominant role than in the visible region due to the major effect of Rayleigh scattering in UV. When Rayleigh scattering was removed, ALH had no effect in both the UV and visible regions of the spectrum.
5. OMI-MODIS method was validated using cruise data from the ICARB and W-ICARB campaigns in the Arabian Sea and Bay of Bengal. The difference between OMI SSA and SSA from cruise measurements despite being small is statistically significant. OMI-MODIS SSA is better constrained and is closer to the cruise measurements
6. It is seen that the OMI overestimates SSA when absorbing aerosols were detected by OMI-MODIS and the cruise measurements.

Aerosol type and aerosol layer height play a very important role in the retrieval of aerosol properties. Without the assumption of aerosol type or height, OMI-MODIS is able to detect absorbing aerosols much better than OMI. Hence this algorithm is useful over regions dominated by absorbing aerosols like Bay of Bengal during winter. The importance of aerosol height is clearly demonstrated by SBDART model and the validation with ground-based measurements highlighted the role of aerosol type. However, an accurate comparison and validation of such retrieval algorithms can be possible only when there are more ground-based observations available in the UV spectrum on a larger spatial and temporal scale.

Acknowledgements

The authors gratefully acknowledge the NOAA Air Resources Laboratory (ARL) for the

483 provision of the HYSPLIT transport and dispersion model used in this publication. The authors
484 are grateful to NASA data and services centre.

485 **References**

486 Bergstrom, R.W., Pilewskie, P., Russell, P.B., Redemann, J., Bond, T.C., Quinn, P.K., and Sierau,
487 B.: Spectral absorption properties of atmospheric aerosols, Atmos. Chem. Phys., 7, 5937-
488 5943, 2007.

489 Bond, T.C., and Sun, H.: Can reducing black carbon emissions counteract global warming?,
490 Environ. Sci. Technol., 39(16), 5921-5926, 2005.

491 Bond, T.C., and Bergstrom, R.W.: Light absorption by carbonaceous particles: An investigative
492 review, Aerosol Sci. Tech., 40(1), 27-67, doi:10.1080/02786820500421521, 2006.

493 Bond, T.C., Doherty, S.J., Fahey, D.W., Forster, P.M., Bernsten, T., De Angelo, B.J., Flanner,
494 M.G., Ghan, S., Karcher, B., Koch, D., Kinne, S., Kondo, Y., Quinn, P.K., Sarofim, M.C.,
495 Schultz, M., Venkataraman, C., Zhang, H., Zhang, S., Bellouin, N., Guttikunda, S.K.,
496 Hopke, P.K., Jacobson, M.Z., Kaiser, J.W., Klimont, Z., Lohmann, U., Schwarz, J.P.,
497 Shindell, D., Storelvmo, T., Warren, S.G., and Zender, C.S.: Bounding the role of black
498 carbon in the climate system: A scientific assessment, J. Geophys. Res., 118(11), 5380-
499 5552, doi:10.1002/jgrd.50171, 2013.

500 Chand, D., Wood, R., Anderson, T.L., Satheesh, S.K., and Charlson, R.J.: Satellite-derived direct
501 radiative effect of aerosols dependent on cloud cover, Nat. Geosci., 2, 181–184,
502 doi:10.1038/ngeo437, 2009.

503 Chung, S.H., and Seinfeld, J.H.: Global distribution and climate forcing of carbonaceous
504 aerosols, J. Geophys. Res., 107(D19), 4407, doi:10.1029/2001JD001397, 2002.

505 Cooke, W.F., and Wilson, J.J.N.: A global black carbon aerosol model, J. Geophys. Res., 101,

19395-19410, doi:10.1029/96JD00671, 1996.

Dey, S., and Di Girolamo, L.: A climatology of aerosol optical and microphysical properties over the Indian subcontinent from 9 years (2000–2008) of Multiangle Imaging Spectroradiometer (MISR) data, J. Geophys. Res., 115, D15204, doi:10.1029/2009JD013395, 2010.

Di Girolamo, L., Bond, T.C., Bramer, D., Diner, D.J., Fettinger, F., Kahn, R.A., Mrtonchik, J.V., Ramana, M.V., Ramanathan, V., and Rasch, P.J.: Analysis of Multi-angle Imaging SpectroRadiometer (MISR) aerosol optical depths over greater India during winter 2001-2004, Geophys. Res. Lett., 31(23), L23115, doi:10.1029/2004GL021273, 2004.

Diner, D.J., Beckert, J.C., Reilly, T.H., Bruegge, C.J., Conel, J.E., Kahn, R.A., Martonchik, J.V., Ackerman, T.P., Davies, R., Gerstl, S.A.W., Gordon, H.R., Muller, J.-P., Myneni, R.B., Sellers, P.J., Pinty, B., and Verstraete, M.M.: Multi-angle Imaging SpectroRadiometer (MISR) instrument description and experiment overview, IEEE T GEOSCI REMOTE, 36(4), 1072-1087, doi:10.1109/36.700992, 1998.

Dubovik, O., and King, M.D.: A flexible inversion algorithm for retrieval of aerosol optical properties from Sun and sky radiance measurements, J. Geophys. Res., 105(D16), 20673-20696, doi:10.1029/2000JD900282, 2000.

Dubovik, O., Holben, B.N., Eck, F.T., Smirnov, A., Kaufman, Y.J., King, M.D., Tanre, D., and Slutsker, I.: Variability of absorption and optical properties of key aerosol types observed in worldwide locations, J. Atmos. Sci., 59(3), 590-608, doi:10.1175/1520-0469(2002)059<0590:VOAAOP>2.0.CO;2, 2002.

Eck, T.F., Holben, B.N., Slutsker, I., and Setzer, A.: Measurements of irradiance attenuation and estimation of aerosol single scattering albedo for biomass burning aerosols in Amazonia, J.

529 Geophys. Res., 103(D24), 31865-31878, doi:10.1029/98JD00399, 1998.
530 Gasso, S., and Torres, O.: The role of cloud contamination, aerosol layer height and aerosol
531 model in the assessment of the OMI near-UV retrievals over the ocean, Atmos. Meas.
532 Tech., 9, 3031-3052, doi:10.5194/amt-9-3031-2016, 2016.
533 Hansen, J., Sato, M., and Ruedy, R.: Radiative forcing and climate response, J. Geophys. Res.-
534 Atmos., 102(D6), 6831-6864, doi:10.1029/96JD03436, 1997.
535 Harriss, R.C., Browell, E.V., Sebacher, D.I., Gregory, G.L., Hinton, R.R., Beck, S.M., McDougal,
536 D.S., and Shipley, S.T.: Atmospheric transport of pollutants from North America to the
537 North Atlantic Ocean, Nature, 308, 722-724, doi:10.1038/308722a0, 1984.
538 Haywood, J.M., Roberts, D.L., Slingo, A., Edwards, J.M., and Shine, K.P.: General circulation
539 model calculations of the direct radiative forcing by anthropogenic sulphate and fossil-fuel
540 soot aerosol, J. Clim., 10, 1562-1577, doi:10.1175/1520-
541 0442(1997)010<1562:GCMCOT>2.0.CO;2, 1997.
542 Heintzenberg, J., Charlson, R.J., Clarke, A. D., Liousse, C., Ramaswamy, V., Shine, K.P.,
543 Wendish, M., and Helas, G.: Measurements and modelling of aerosol single-scattering
544 albedo: Progress, problems and prospects, Contrib. Atmos. Phys., 70(4), 249– 263, 1997.
545 Herman, B.M., Browning, R.S., and De Luisi, J.J.: Determination of the effective imaginary term
546 of the complex refractive index of atmospheric dust by remote sensing: the diffuse-direct
547 radiation method, J. Atmos. Sci., 32, 918-925, doi:10.1175/1520-
548 0469(1975)032<0918:DOTEIT>2.0.CO;2, 1975.
549 Herman, J.R., Bhartia, P.K., Torres, O., Hsu, C., Seftor, C., and Celarier, E.: Global distribution
550 of UV-absorbing aerosols from Nimbus 7/TOMS data, J. Geophys. Res.-Atmos., 102(D14),
551 16911-16922, doi:10.1029/96JD03680, 1997.

552 Horvath, H.: Atmospheric light absorption- a review, Atmos. Environ. A-Gen., 27(3), 293-317,
553 doi:10.1016/0960-1686(93)90104-7, 1993.
554 Intergovernmental Panel on Climate Change (IPCC) (2013), The physical science basis:
555 Contribution of Working Group I to the Fifth Assessment Report of the Intergovernmental
556 Panel on Climate Change, In: Climate Change (2013), Stocker, T.F., D. Qin, G.K. Plattner,
557 M. Tignor, S.K. Allen, J. Boschung, A. Nauels, Y. Xia, V. Bex, and P.M. Midgley (eds),
558 Cambridge University, Press: Cambridge, United Kingdom and New York, NY, USA 1535
559 pp, doi:10.1017/CBO9781107415324.
560 Jethva, H., Torres O., and Ahn C.: Global assessment of OMI aerosol single-scattering albedo
561 using ground-based AERONET inversion, J. Geophys. Res.-Atmos., 119(14), 9020-9040,
562 doi:10.1002/2014JD021672, 2014.
563 Johnson, B.T., Shine, K.P., and Forster, P.M.: The semi-direct aerosol effect: Impact of absorbing
564 aerosols on marine stratocumulus, Q. J. Roy. Meteor. Soc., 130, 1407-1422,
565 doi:10.1256/qj.03.61, 2003.
566 Kaufman, Y.J.: Satellite sensing of aerosol absorption, J. Geophys. Res., 92, 4307-4317,
567 doi:10.1029/JD092iD04p04307, 1987.
568 Kaufman, Y.J., Tanre, D., and Boucher, O.: A satellite view of aerosols in the climate system,
569 Nature, 419, 215-223, doi:10.1038/nature01091, 2002a.
570 Kaufman, Y.J., Martins, J.V., Remer, L.A., Schoeberl, M.R., and Yamasoe, M.A.: Satellite
571 retrieval of aerosol absorption over the oceans using sunglint, Geophys. Res. Lett., 29(19),
572 34-1 – 34-4, doi:10.1029/2002GL015403, 2002b.
573 Kaufman, Y.J., Koren, I., Remer, L.A., Tanre, D., Ginoux, P., and Fan, S.: Dust transport and
574 deposition observed from the Terra-Moderate Resolution Imaging Spectroradiometer

(MODIS) spacecraft over the Atlantic Ocean, J. Geophys. Res., 110, D10S12, doi:10.1029/2003JD004436, 2005.

Kim, S-W., Yoon, S-C., Jefferson, A., Won, J-G., Dutton, E.G., Ogren, J.A., and Anderson T.L.: Observation of enhanced water vapour in Asian dust layer and its effect on atmospheric radiative heating rates, Geophys. Res. Lett., 31(18), doi:10.1029/2004GL020024, 2004.

King, M.D.: Determination of the ground albedo and the index of absorption of atmospheric particulates by remote sensing. Part II: Application, J. Atmos. Sci., 36, 1072-1083, doi:10.1175/1520-0469(1979)036<1072:DOTGAA>2.0.CO;2, 1979.

Krishnamurti, T.N., Jha, B., Prospero J., Jayaraman, A., and Ramanathan, V.: Aerosol and pollutant transport and their impact on radiative forcing over the tropical Indian Ocean during the January – February 1996 pre-INDOEX cruise, Tellus B, 50(5): 521–542, doi:10.1034/j.1600-0889.1998.00009.x, 1998.

Kumar, K.R., Sivakumar, Reddy, R.R., and Gopal, K.R.: Ship-borne measurements of columnar and surface aerosol loading over the Bay of Bengal during W-ICARB campaign: role of airmass transport. Latitudinal and Longitudinal Gradients, Aerosol Air Qual Res., 13, 818–837, doi:10.4209/aaqr.2012.08.0225, 2013.

Lawrence, M.G., and Lelieveld, J.: Atmospheric pollutant outflow from southern Asia: a review, Atmospheric Chemistry and Physics, 10, 11017-11096, doi:10.5194/acp-10-11017-2010, 2010.

Levy, R.C., Remer, L.A., Tanre, D., Kaufman, Y.J., Ichoku, C., Holben, B.N., Livingston, J.M., Russell, P.B., and Maring, H.: Evaluation of the Moderate-Resolution Imaging Spectroradiometer (MODIS) retrievals of dust aerosol over the ocean during PRIDE, J. Geophys. Res., 108(D19), 8594, doi:10.1029/2002JD002460, 2003.

598 Liao, H., and Seinfeld, J.H.: Radiative forcing by mineral dust aerosols: Sensitivity to key
599 variables, J. Geophys. Res.-Atmos., 103(D24), 31637-31645, doi:10.1029/1998JD200036,
600 1998.
601 Meloni, D., di Sarra, A., di Lorio, T., and Fiocco, G.: Influence of the vertical profile of Saharan
602 dust on the visible direct radiative forcing, J. Quant. Spectrosc. Ra., 93(4), 397-413,
603 doi:10.1016/j.jqsrt.2004.08.035, 2005.
604 Menon, S., Hansen, J., Nazarenko, L., and Luo, Y.: Climate effects of black carbon aerosols in
605 China and India, Science, 297(5590), 2250-2253, doi:10.1126/science.1075159, 2002.
606 Mishra, A.K., Koren, I., and Rudich, Y.: Effect of aerosol vertical distribution on aerosol-
607 radiation interaction: A theoretical prospect, Heliyon, e00036,
608 doi:10.1016/j.heliyon.2015.e00036, 2015.
609 Moorthy, K.K., Babu, S.S., and Satheesh, S.K.: Aerosol spectral optical depths over the Bay of
610 Bengal: role of transport, Geophys. Res. Lett., 30(5): 1249, doi:10.1029/2002GL016520,
611 2003.
612 Moorthy, K.K., Babu, S.S., Sunilkumar, S.V., Gupta, P.K., and Gera, B.S.: Altitude profiles of
613 aerosol BC, derived from aircraft measurements over an inland urban location in India,
614 Geophys. Res. Lett., 31(22), 10.1029/2004GL021336, 2004.
615 Moorthy, K.K., Satheesh, S.K., Babu, S.S., and Dutt, C.B.S.: Integrated campaign for aerosols,
616 gases and radiation budget (ICARB): an overview, J. Earth. Syst. Sci., 117(1), 243-262,
617 doi:10.1007/s12040-008-0029-7, 2008.
618 Moorthy, K.K., Beegum, S.N., Babu, S.S., Smirnov, A., John, S.R., Kumar, K.R., Narasimhulu,
619 K., Dutt, C.B.S., and Nair, V.S.: Optical and physical characteristics of Bay of Bengal
620 aerosols during W-ICARB: spatial and vertical heterogeneities in the marine atmospheric

boundary layer and in the vertical column, J. Geophys. Res., 115(D24): D24213, doi:10.1029/2010JD014094, 2010.

Moosmuller, H., Chakrabarty, R.K., and Arnott, W.P.: Aerosol light absorption and its measurement: A review, J. Quant. Spectrosc. Ra., 110(11), 844-878, doi:10.1016/j.jqsrt.2009.02.035, 2009.

Morris, V., Colon, P.C., Nalli, N.R., Joseph, E., Armstrong, R.A., Detres, Y., Goldberg, M.D., Minnett, P.J., and Lumpkin, R.: Measuring Trans-Atlantic aerosol transport from Africa, EOS Trans. AGU, 87(50), 565-571, doi:10.1029/2006EO500001, 2006.

Myhre, G., Stordal, F., Restad, K., and Isaksen, I.S.A.: Estimation of the direct radiative forcing due to sulphate and soot aerosols, Tellus, 50B, 463-477, 1998.

Narasimhan, D., and Satheesh, S.K.: Estimates of aerosol absorption over India using multi-satellite retrieval, Ann. Geophys., 31, 1773-1778, doi:10.5194/angeo-31-1773-2013, 2013.

Pease, P.P., Tchakerian, V.P., and Tindale, N.W.: Aerosols over the Arabian Sea: geochemistry and source areas for Aeolian desert dust, J. Arid Environ., 39(3), 477-496, doi:10.1006/jare.1997.0368, 1998.

Podgorny, I.A., and Ramanathan, V.: A modeling study of the direct effect of aerosols over the tropical Indian Ocean, J. Geophys. Res., 106(D20): 24097–24105, doi:10.1029/2001JD900214, 2001.

Prospero, J.M., and Carlson, T.N.: Vertical and areal distribution of Saharan dust over the western equatorial north Atlantic Ocean, J. Geophys. Res., 77(27), 5255-5265, doi:10.1029/JC077i027p05255, 1972.

Prospero, J.M.: Saharan dust transport over the North Atlantic Ocean and Mediterranean: An overview, In: The Impact of Desert Dust Across the Mediterranean, Guerzoni S., Chester

R. (Eds.), 133-151, doi:10.1007/978-94-017-3354-0_13, 1996.

Rajeev, K., Ramanathan, V., and Meywerk, J.: Regional aerosol distribution and its long-range transport over the Indian Ocean, J. Geophys. Res.-Atmos., 105(D2), 2029-2043, doi:10.1029/1999JD900414, 2000.

Ramanathan, V., Crutzen, P.J., Kiehl, J.T., and Rosenfield, D.: Aerosols, climate and the hydrological cycle, Science, 294(5549): 2119–2124, doi:10.1126/science.1064034, 2001.

Remer, L. A., Kaufman, Y. J., Tanre, D., Mattoo, S., Chu, D. A., Martins, J. V., Li, R. R., Ichoku, C., Levy, R. C., Kleidman, R. G., Eck, T. F., Vermote, E., and Holben, B. N.: The MODIS aerosol algorithm, products, and validation, J. Atmos. Sci., 62, 947–973, doi:10.1175/JAS3385.1, 2005.

Ricchiazzi, P., Yang, S., Gautier, C., and Sowle, D.: SBDART: a research and teaching software tool for plane-parallel radiative transfer in the earth's atmosphere, B. Am. Meteorol. Soc. 79(10): 2101–2114, doi:10.1175/1520-0477(1998)079<2101: SARATS>2.0.CO;2, 1998.

Satheesh, S.K.: Aerosols and climate, Resonance, 7(4), 48-59, doi:10.1007/BF02836138, 2002.

Satheesh, S.K., and Moorthy, K.K.: Radiative effects of natural aerosols: a review, Atmos. Environ., 39(11): 2089–2110, doi:10.1016/j.atmosenv.2004.12.029, 2005.

Satheesh, S.K., Srinivasan, J., and Moorthy, K.K.: Spatial and temporal heterogeneity in aerosol properties and radiative forcing over Bay of Bengal: Sources and role of aerosol transport, J. Geophys. Res., 111(D8): D08202, doi:10.1029/2005JD006374, 2006.

Satheesh, S.K., Moorthy, K.K., Babu, S.S., Vinoj, V., and Dutt, C.B.S.: Climate implications of large warming by elevated aerosol over India, Geophys. Res. Lett., 35(19), doi:10.1029/2008GL034944, 2008.

Satheesh, S.K., Torres, O., Remer, L.A., Babu, S.S., Vinoj, V., Eck, T.F., Kleidman, R.G., and

667 Holben, B.N.: Improved assessment of aerosol absorption using OMI-MODIS joint
668 retrieval, J. Geophys. Res., 114, D05209, doi:10.1029/2008JD011024, 2009.
669 Satheesh, S.K., Vinoj, V., and Moorthy, K.K.: Assessment of aerosol radiative impact over
670 oceanic regions adjacent to Indian subcontinent using multi-satellite analysis, Adv.
671 Meteorol., 2010, Article ID 139186, pp 13., doi:10.1155/2010/139186, 2010.
672 Seinfeld, J.H., and Pandis, S.N.: Atmospheric Chemistry and Physics: From air pollution to
673 climate change, 2nd Ed., 1232 pp, John Wiley & Sons, Inc., Hobkoben, New Jersey, 2006.
674 Sirocko, F., and Sarnthein, M.: Wind-borne deposits in the northwestern Indian Ocean: Record of
675 Holocene sediments versus modern satellite data, In: Paleoclimatology and
676 Paleometeorology: modern and past patterns of global atmospheric transport, Leinen M.,
677 Sarnthein M. (Eds), 401-433, Amsterdam: Kluwer Academic Publishers, 1989.
678 Stephens, G.L., Vane, D.G., Boain, R.J., Mace, G.G., Sassen, K., Wang, Z., Illingworth, A.J.,
679 O'Connor, E.J., Rossow, W.B., Durden, S.L., Miller, S.D., Austin, R.T., Benedetti, A.,
680 Mitrescu, C., and CloudSat Science Team: The CloudSat mission and the A-Train: A new
681 dimension of space-based observations of clouds, precipitation, B. Am. Meteorol. Soc., 83,
682 1771-1790, doi:10.1175/BAMS-83-12-1771, 2002.
683 Tanre, D., Kaufman, Y.J., Herman, M., and Mattoo, S.: Remote sensing of aerosol properties
684 over oceans using the MODIS/EOS spectral radiances, J. Geophys. Res., 102(D14),
685 16971–16988, 1997.
686 Tindale, N.W., and Pease, P.P.: Aerosols over the Arabian Sea: Atmospheric transport pathways
687 and concentrations of dust and sea salt, Deep-Sea Res. Pt. II, 46(8-9), 1577-1595,
688 doi:10.1016/S0967-0645(99)00036-3, 1999.
689 Torres, O., Bhartia, P. K., Herman, J. R., and Ahmad, Z.: Derivation of aerosol properties from

satellite measurements of backscattered ultraviolet radiation. Theoretical Basis, J. Geophys. Res., 103(D14), 17099–17110, 1998.

Torres, O., Decae, R., Veefkind, J.P., and de Leeuw, G.: OMI aerosol retrieval algorithm, in OMI Algorithm Theoretical Basis Document: Clouds, Aerosols, and Surface UV Irradiance, 3, V2, OMIATBD- 03, edited by P. Stammes, pp. 47 – 71, NASA Goddard Space Flight Cent., Greenbelt, Md, 2002. (http://eospso.gsfc.nasa.gov/eos_homepage/for_scientists/atbd/docs/OMI/ATBD-OMI-03.pdf)

Torres, O., Bhartia, P.K., Sinyuk, A., Welton, E.J., and Holben, B.: Total Ozone Mapping Spectrometer measurements of aerosol absorption from space: Comparison to SAFARI 2000 ground-based observations, J. Geophys. Res., 110(D10), doi:10.1029/2004JD004611, 2005.

Torres, O., Tanskanen, A., Veihelmann, B., Ahn, C., Braak, R., Bhartia, P.K., Veefkind, P., and Levelt, P.: Aerosols and surface UV products from Ozone Monitoring Instrument observations: An overview, J. Geophys. Res., 112, D24S47, doi:10.1029/2007JD008809, 2007.

Torres, O., Ahn, C., and Chen, Z.: Improvements to the OMI near-UV aerosol algorithm using A-train CALIOP and AIRS observations, Atmos. Meas. Tech., 6, 3257-3270, doi:10.5194/amt-6-3257-2013, 2013.

Van de Hulst, H.C.: Light scattering by small particles, 496 pp., Dover publications, New York, 1981.

Wells, K.C., Martins, J.V., Remer, L.A., Kreidenweis, S.M., and Stephens, G.L.: Critical reflectance derived from MODIS: Application for the retrieval of aerosol absorption over

desert regions, J. Geophys. Res., 117(D3), doi:10.1029/2011JD016891, 2012.

Zhu, L., Martins, J.V., and Remer, L.A.: Biomass burning aerosol absorption measurements with MODIS using the critical reflectance method, J. Geophys. Res., 116(D7), doi:10.1029/2010JD015187, 2011.

Zuluaga, M.D., Webster, P.J., and Hoyos, C.D.: Variability of aerosols in the tropical Atlantic Ocean relative to African Easterly Waves and their relationship with atmospheric and oceanic environments, J. Geophys. Res., 117(D16), doi:10.1029/2011JD017181, 2012.

Atmos. Chem. Phys. Discuss., https://doi.org/10.5194/acp-2018-564
Manuscript under review for journal Atmos. Chem. Phys.
Discussion started: 16 July 2018

Atmospheric Chemistry and Physics Discussions

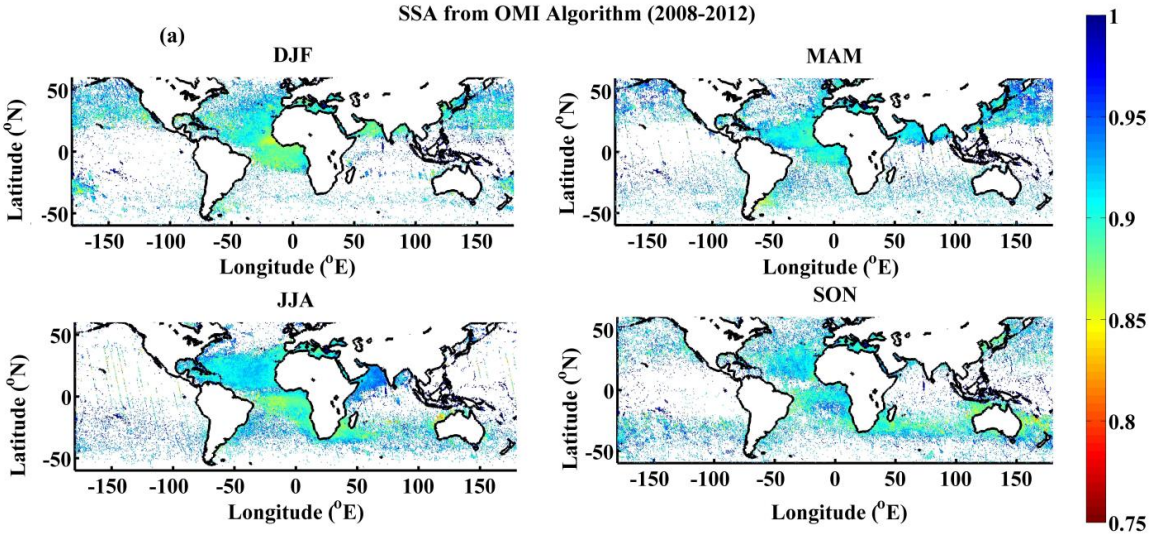

733

734 **Figure 1a.** Spatial distribution of SSA retrieved by OMI

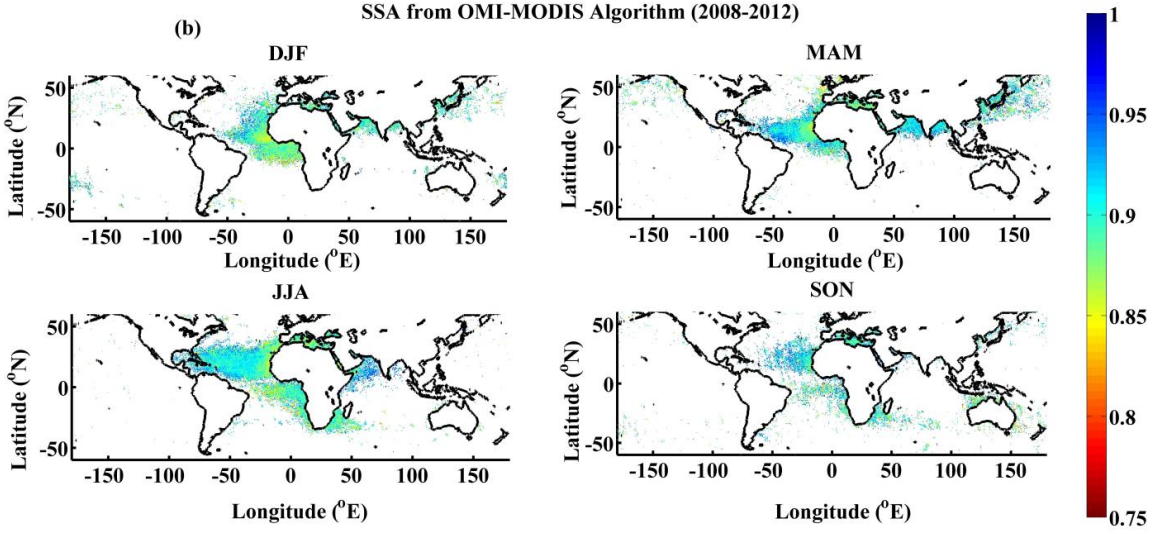

735

736 **Figure 1b.** Spatial distribution of SSA retrieved by OMI-MODIS

Atmos. Chem. Phys. Discuss., https://doi.org/10.5194/acp-2018-564
Manuscript under review for journal Atmos. Chem. Phys.
Discussion started: 16 July 2018

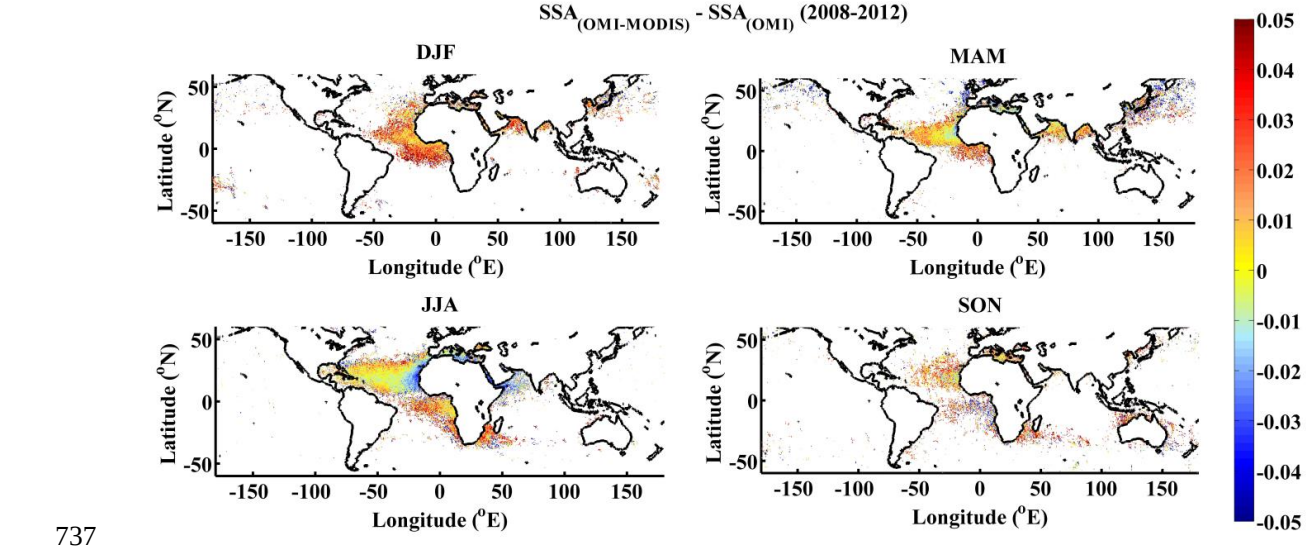

Figure 2. Spatial distribution of difference in SSA retrievals

Atmos. Chem. Phys. Discuss., https://doi.org/10.5194/acp-2018-564
Manuscript under review for journal Atmos. Chem. Phys.
Discussion started: 16 July 2018

Atmospheric Chemistry and Physics Discussions

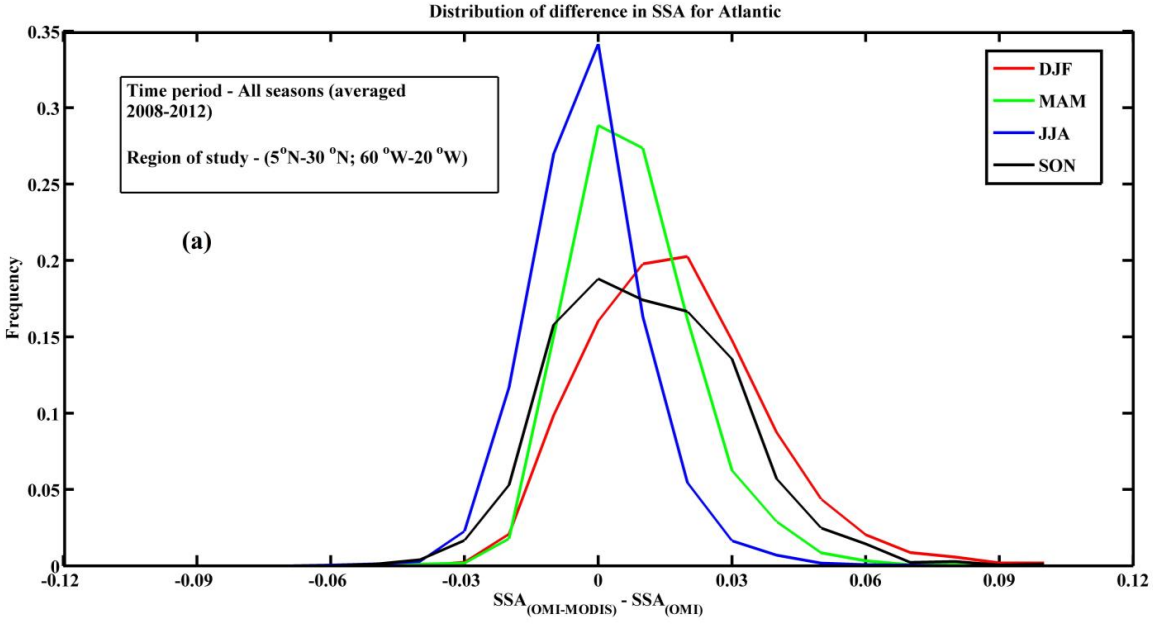

745

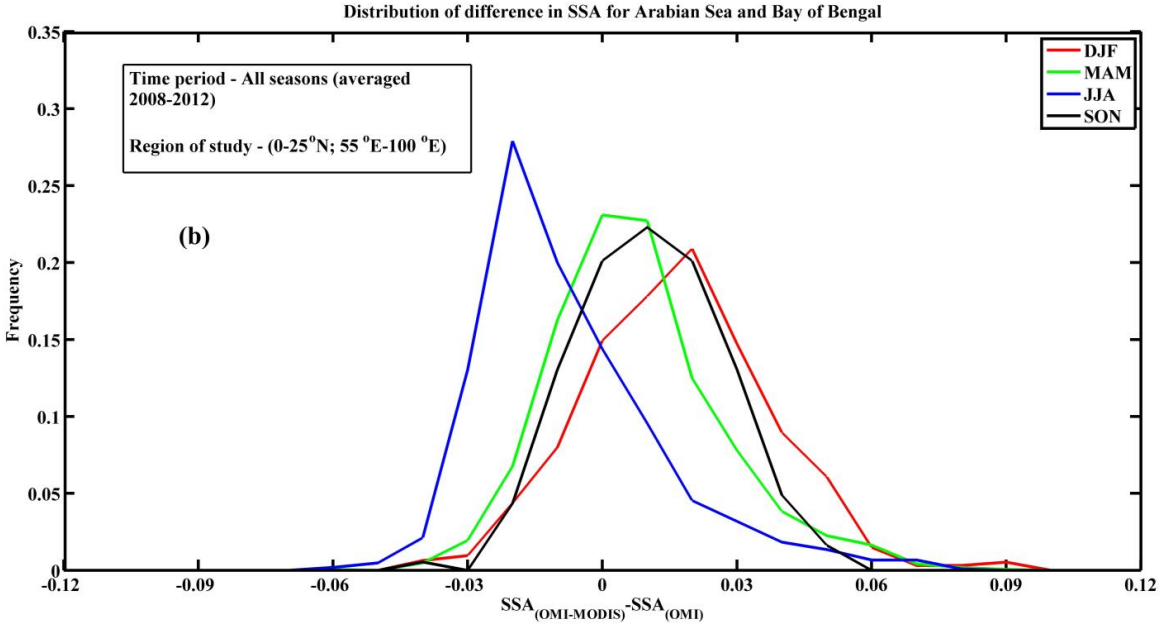

746

747 **Figure 3.** Distribution of difference in SSA for all seasons averaged over 2008-2012 over a)

748 Atlantic and b) Arabian Sea and Bay of Bengal

Atmos. Chem. Phys. Discuss., https://doi.org/10.5194/acp-2018-564
Manuscript under review for journal Atmos. Chem. Phys.
Discussion started: 16 July 2018

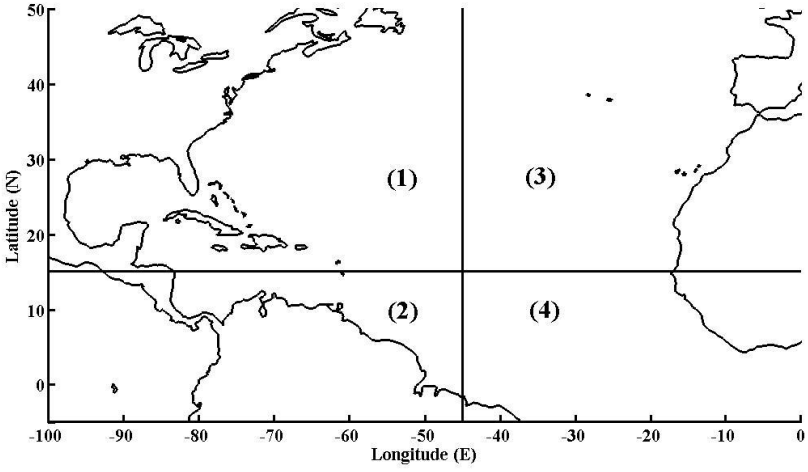

749

750 **Figure 4.** Regions representing the various aerosol sources over Atlantic Ocean. 1) North
751 America, 2) Central/South America, 3) North Africa and 4) Southern Africa.

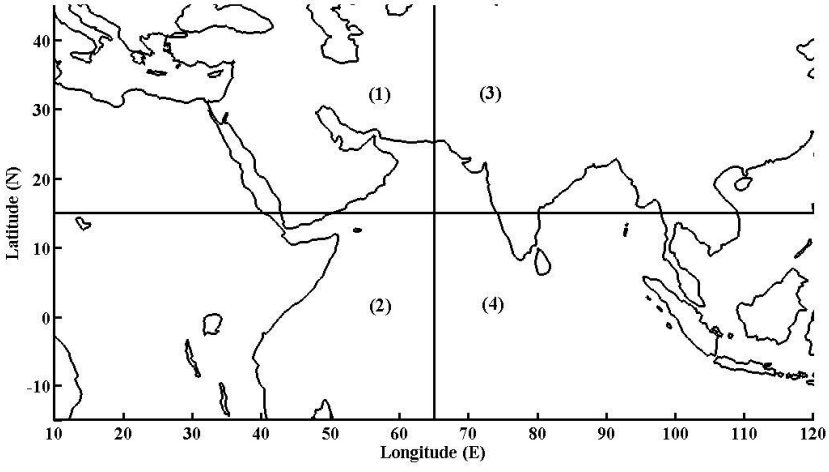

752

753 **Figure 5.** Regions representing the various aerosol sources over Arabian Sea. 1) Arabian
754 Peninsula and North Africa, 2) Southern Africa, 3) Indian sub-continent and 4) Indian Ocean and
755 Southeast Asia.

Atmos. Chem. Phys. Discuss., https://doi.org/10.5194/acp-2018-564
Manuscript under review for journal Atmos. Chem. Phys.
Discussion started: 16 July 2018

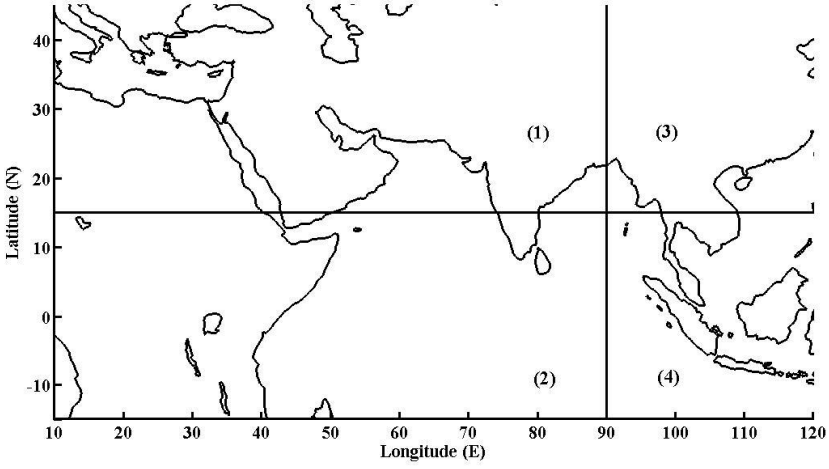

Figure 6. Regions representing the various aerosol sources over Bay of Bengal. 1) India/Arabian Peninsula, 2) Indian Ocean, 3) North/Northeast India and East Asia and 4) Southeast Asia.

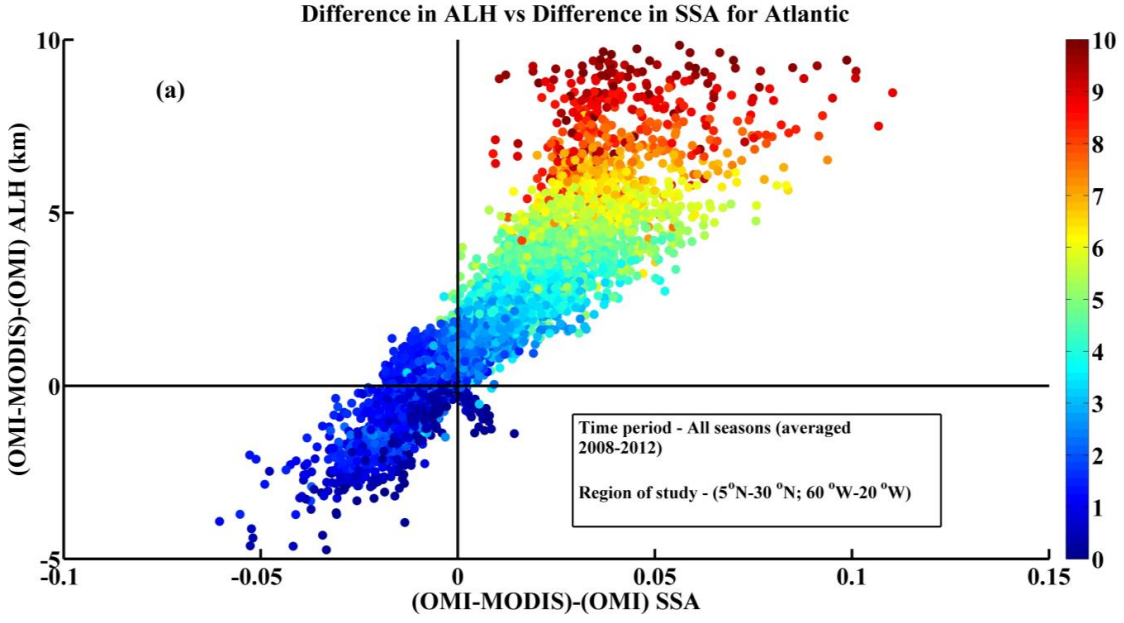

Atmos. Chem. Phys. Discuss., https://doi.org/10.5194/acp-2018-564
Manuscript under review for journal Atmos. Chem. Phys.
Discussion started: 16 July 2018

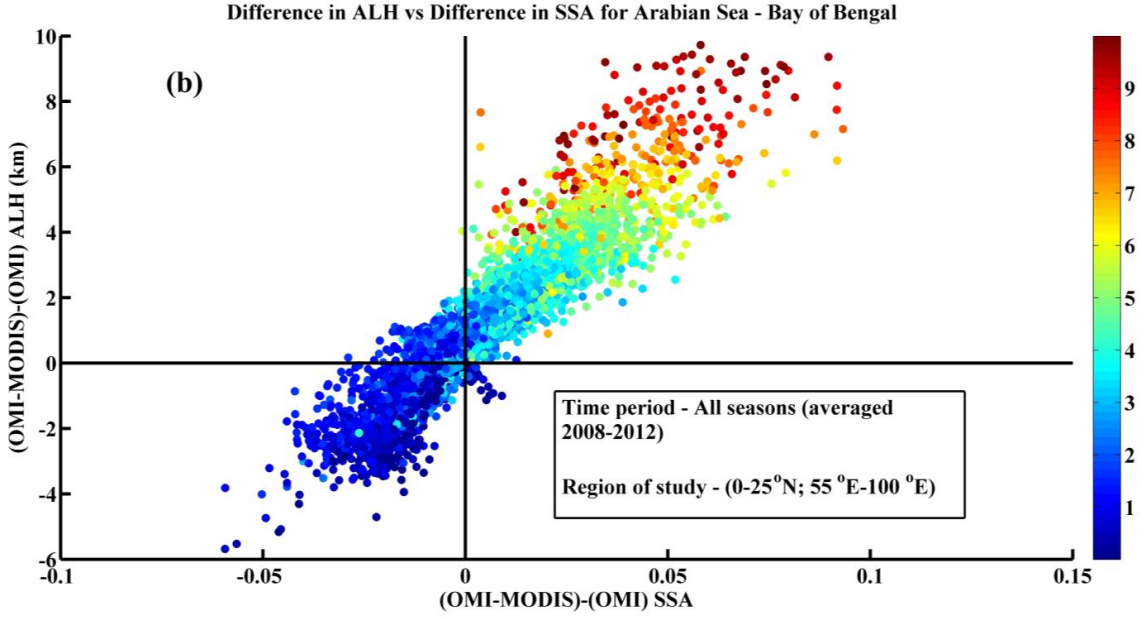

760

761 **Figure 7.** Difference in aerosol layer height (ALH) between OMI-MODIS and OMI vs.
762 difference in SSA over a) Atlantic and b) Arabian Sea and Bay of Bengal. The colorbar
763 represents ALH estimated by OMI-MODIS algorithm. At lower height (dark blue circles) OMI
764 assumes ALH greater than that of OMI-MODIS and results in overestimation of SSA.

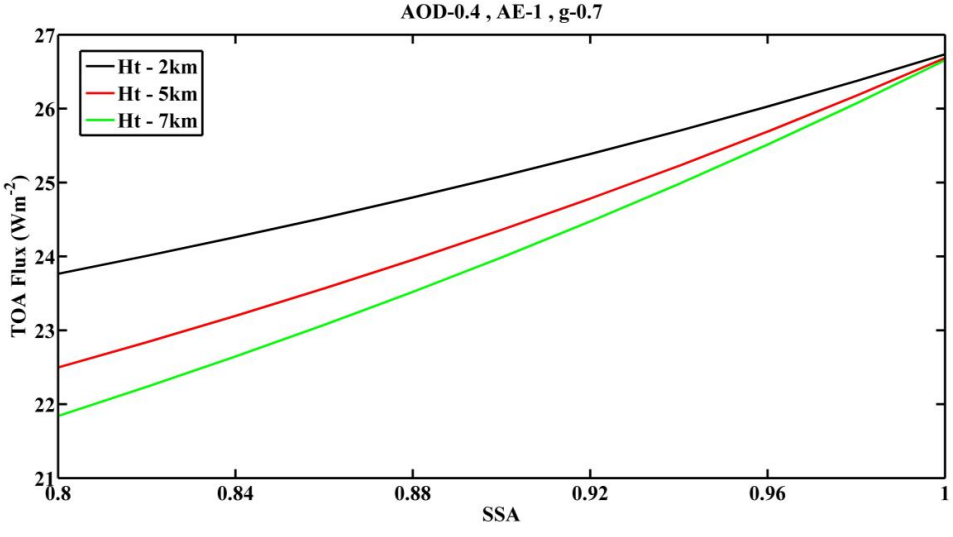

765

Atmos. Chem. Phys. Discuss., https://doi.org/10.5194/acp-2018-564
Manuscript under review for journal Atmos. Chem. Phys.
Discussion started: 16 July 2018

766 **Figure 8.** TOA flux calculated from SBDART for different SSA and ALH for UV (300-400nm)

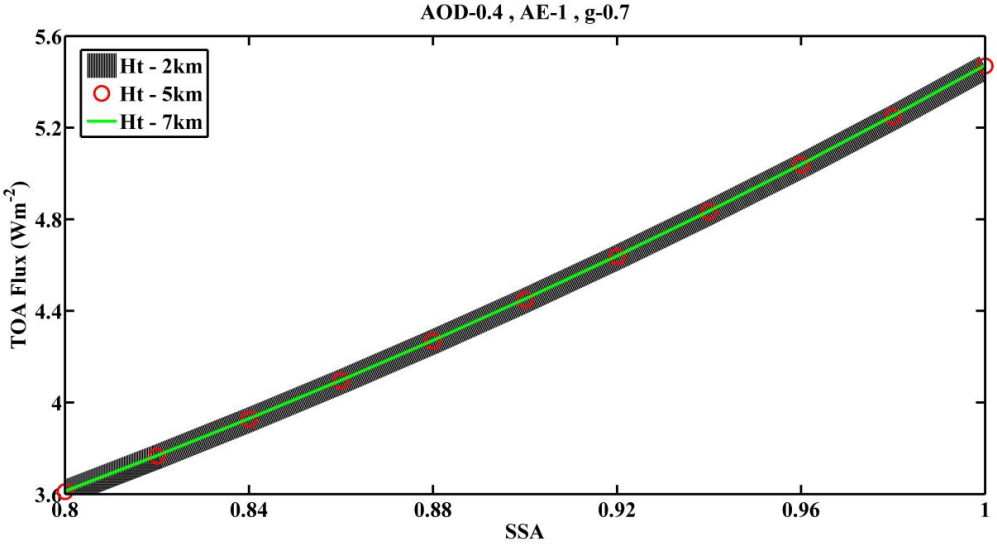

767

768 **Figure 9.** TOA flux calculated from SBDART for different SSA and ALH with Rayleigh

769 scattering removed for UV (300-400nm)

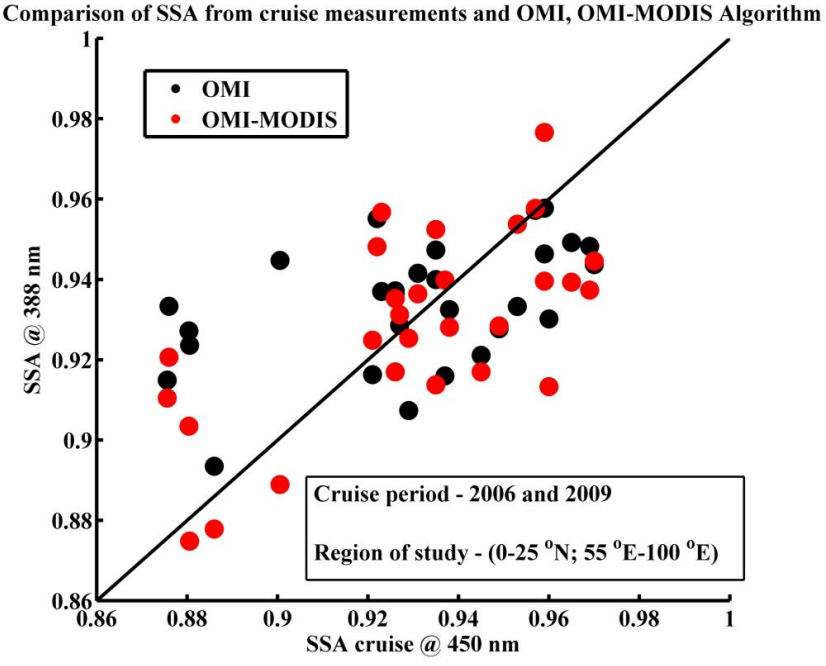

770

Atmos. Chem. Phys. Discuss., https://doi.org/10.5194/acp-2018-564
Manuscript under review for journal Atmos. Chem. Phys.
Discussion started: 16 July 2018

Atmospheric Chemistry and Physics Discussions

771 **Figure 10.** Comparison of SSA_{OMI}, $SSA_{OMI\text{-}MODIS}$ with cruise measurements spatially averaged

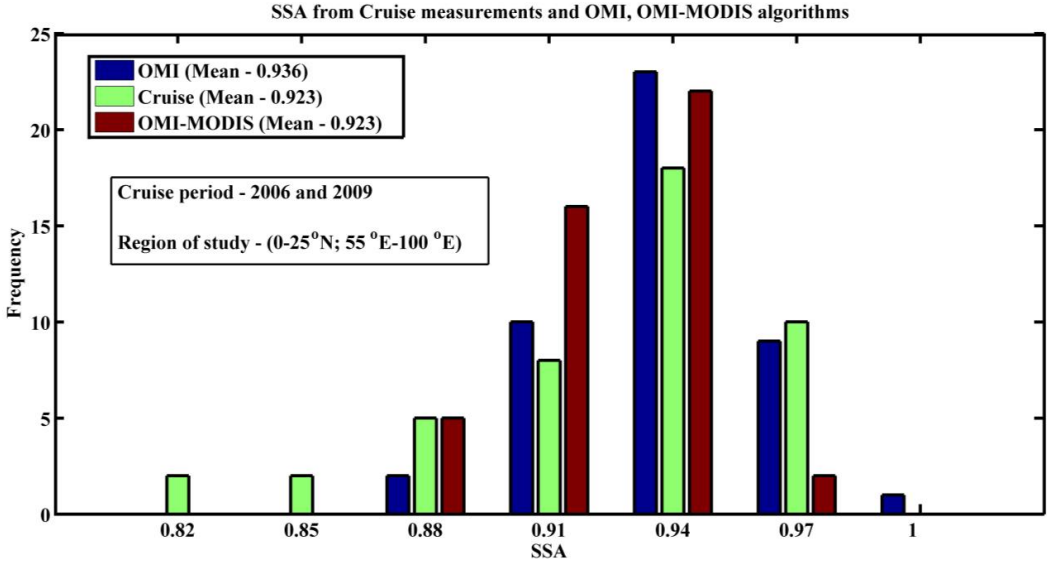

772

773 **Figure 11.** Distribution of SSA from OMI-MODIS, OMI and cruise measurements.

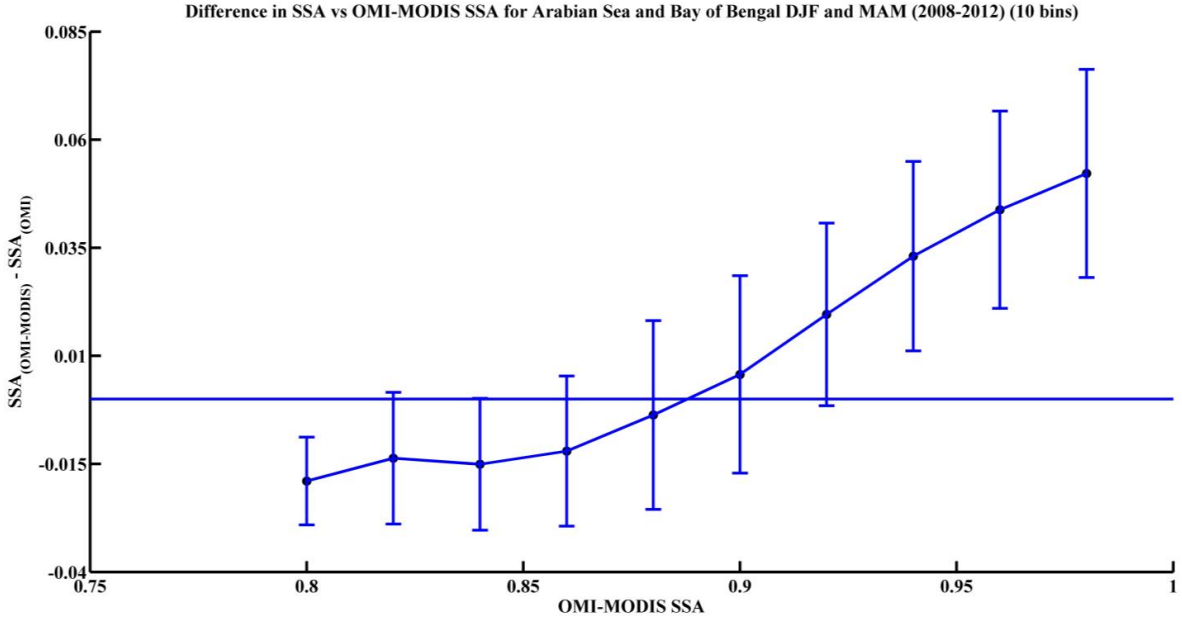

774

775 **Figure 12.** Difference in SSA from OMI-MODIS and OMI Vs SSA from OMI-MODIS. OMI

776 overestimates SSA when absorbing aerosols are detected by OMI-MODIS.

777

778

779

780

781

References	Method	Technique	Limitation
Herman et al., 1975; King, 1979; Eck et al., 1998; Dubovik and King, 2000; Torres et al., 2005	Ground-based observations	Inverse methods measurements of solar radiances and/or aerosol properties along with radiative transfer calculations	Measurements are spatially and temporally constrained
Dubovik et al., 2002	Global network – Aerosols Robotic Network (AERONET)	Inverse technique using near-real time measured direct and diffuse radiation	Only land-based, low coverage over remote oceanic regions

Kaufman, 1987; Zhu et al., 2011; Wells et al., 2012	Critical surface reflectance - where the net role of aerosol absorption and scattering becomes independent of aerosol optical thickness and is affected only by SSA	Over varying surface reflectance, the radiance difference between clear and hazy skies is measured using satellite images	Limited spatial variability of surface reflectance. Works only for few cases where there are large amount absorbing aerosols present
Kaufman et al., 2002b	Retrieve SSA in visible wavelengths	Sun-glint is used as a bright background to differentiate role of scattering from aerosol absorption	Only limited scenarios present and does not work on land when absorbing aerosols are present (Torres et al., 2005).
Diner et al., 1998; Remer et al., 2005	Multi Angle Imaging Spectroradiometer (MISR) and Moderate Resolution Imaging Spectroradiometer (MODIS)	Retrieves AOD and SSA in the visible and infrared region of solar spectrum	Surface reflectance influences the retrievals

Atmos. Chem. Phys. Discuss., https://doi.org/10.5194/acp-2018-564
Manuscript under review for journal Atmos. Chem. Phys.
Discussion started: 16 July 2018

Herman et al., 1997; Torres et al., 1998	Total Ozone Mapping Spectrometer (TOMS)	Aerosol index parameter is highly sensitive to the Rayleigh scattering thus acting as a bright background in the UV regime	Large pixel size prone to cloud contamination
Torres et al., 2002	Ozone Monitoring Instrument (OMI)	Similar technique as TOMS. Pre-defined aerosol models used.	Sensitive to aerosol layer height and still prone to cloud contamination

Table 1. Ground-based and Satellite-based indirect methods to retrieve SSA

Seasons / **Regions**		**1**		**2**		**3**		**4**	
		2009	**2010**	**2009**	**2010**	**2009**	**2010**	**2009**	**2010**
DJF	500m	38%	40%	0%	0%	**57%**	**45%**	5%	15%
	1500m	**43%**	**45%**	0%	0%	24%	20%	33%	35%
	2500m	**52%**	**50%**	10%	10%	5%	15%	33%	25%
MAM	500m	9%	19%	0%	0%	**86%**	**62%**	5%	19%
	1500m	**33%**	**38%**	0%	4%	**53%**	**29%**	14%	29%
	2500m	**38%**	**24%**	19%	0%	29%	33%	14%	43%

Atmos. Chem. Phys. Discuss., https://doi.org/10.5194/acp-2018-564
Manuscript under review for journal Atmos. Chem. Phys.
Discussion started: 16 July 2018

Atmospheric Chemistry and Physics Discussions

JJA	500m	5%	5%	0%	0%	**90%**	**90%**	5%	5%
	1500m	9%	5%	0%	0%	**67%**	**76%**	24%	19%
	2500m	0%	5%	0%	0%	**76%**	**76%**	24%	19%
SON	500m	5%	5%	0%	0%	**86%**	**71%**	9%	24%
	1500m	0%	10%	0%	0%	**81%**	**71%**	19%	19%
	2500m	10%	14%	0%	0%	**71%**	**57%**	19%	29%

Table 2. Influence of various aerosol sources over Atlantic Ocean given as percentage of trajectories originating from each source respectively. The maximum influence is given in black bold. The different source regions are explained in text and Fig. 4.

Seasons / **Regions**		**1**	**2**	**3**	**4**
DJF	500m	**57%**	0%	38%	5%
	1500m	**62%**	10%	19%	9%
	2500m	**81%**	14%	0%	5%
MAM	500m	19%	**43%**	19%	19%
	1500m	29%	**29%**	23%	19%
	2500m	**57%**	14%	24%	5%
JJA	500m	0%	24%	0%	**76%**
	1500m	19%	**67%**	0%	14%
	2500m	**62%**	33%	5%	0%

SON	500m	5%	24%	**47%**	24%
	1500m	14%	19%	**48%**	19%
	2500m	**38%**	10%	19%	33%

790

791 **Table 3.** Influence of various aerosol sources over Arabian Sea given as percentage of
792 trajectories originating from each source respectively. The maximum influence is given in black
793 bold. The different source regions are explained in text and Fig. 5.

794

Seasons / **Regions**		**1**	**2**	**3**	**4**
DJF	500m	**72%**	0%	14%	14%
	1500m	**48%**	14%	10%	28%
	2500m	29%	33%	0%	**38%**
MAM	500m	19%	**48%**	0%	33%
	1500m	**57%**	29%	20%	14%
	2500m	**71%**	24%	0%	5%
JJA	500m	0%	**100%**	0%	0%
	1500m	5%	**95%**	0%	0%
	2500m	14%	**81%**	0%	5%
SON	500m	5%	**52%**	33%	10%
	1500m	5%	**43%**	**43%**	9%
	2500m	5%	**33%**	29%	**33%**

795

796 **Table 4.** Influence of various aerosol sources over Bay of Bengal given as percentage of
797 trajectories originating from each source respectively. The maximum influence is given in black
798 bold. The different source regions are explained in text and Fig. 6.

799

	OMI	**OMI-MODIS**
Mean SSA (Cruise – 0.923)	0.936	0.923
Std. Dev. (Cruise – 0.04)	0.021	0.021
p- value	0.046	0.981
Confidence Interval	[0.0002, 0.027]	[-0.013,0.013]

800

801 **Table 5.** Comparison of SSA between both the satellite algorithms and cruise measurements

802